Supplementary Materials: The Effect of Adsorption Phenomena on the Transport in Complex Electrolytes

S1. Aqueous ferrofluids used in section 5 of main paper

The aqueous ferrofluids used in the present study are based on maghemite (γ-Fe_2O_3) nanoparticles with an average diameter of 7-8 nm, synthesized following the method developed by Massart (see [1]). The nanoparticles are citrate-coated (with citrate co-ions) and electrostatically stabilized with monovalent counterions of tetrabutyl ammonium ($TBuA^+$) in water at pH 7. The NPs have a negative structural charge Z_{struct} of 130 ± 40 elementary electrostatic charges, partly cancelled by the nearby cations (here, $TBuA^+$) condensed within the NPs' first solvation layers, resulting in a much smaller dynamic effective number of charges $Z^* \sim$ - 33 ± 7, associated to a zeta potential -38 ± 8 mV. In [2,3], the colloidal stability of such dispersions has been tested in a large range of counter-ion and NP concentrations (up to [$TBuA_3Cit$] = 23 mM and ϕ= 3.7%) by Small Angle X-ray Scattering, Dynamic Light Scattering and Rayleigh Forced Scattering. Electrical conductivity and Seebeck coefficient measurements of such dispersions have been realized in [4] in the range $10^{-5} \leq \phi \leq 10^{-2}$ with [$TBuA_3Cit$] $\sim$ 30 mM, associated to a Debye length $\lambda_0 \sim$ 1.0 nm (see Table 1 of Ref. [5] (As recalled in [5], big citrate ions do not behave experimentally as a trivalent electrolyte, but as three independent monovalent electrolytes.)).

S2. Inductively Coupled Plasma measurements

S2.1. ICP principle

Iron concentrations are assessed using an Agilent 7900 quadrupole ICP-MS. ^{56}Fe and ^{57}Fe were measured using a collision-reaction cell with helium gas (5 mL/min) to remove polyatomic interferences. Elemental concentrations estimated with both isotopes are similar considering analytical uncertainties. The most abundant isotope (^{56}Fe) was therefore used to report final elemental concentrations.

A scandium internal-standard is injected after inline mixing with the samples to correct for signal drift and matrix effects. A set of calibration standards, ranging from 0.1 to 500 ppb, is analyzed to confirm and model (through simple linear regression) the linear relationship between signal and concentration. The model is then used to convert measured sample counts to concentrations. Reported uncertainties are calculated using error propagation equations and considering the combination of standard deviation on replicated consecutive signal acquisitions (n = 3), internal-standard ratio and blank subtraction. The non-linear term (internal-standard ratio) is linearized using a first-order Taylor series expansion to

Table S1. Adsorption test on the Pt electrode: Fe in ppb from ICP determinations at the different steps (volume of sample around 10 ml, precisely weighted. RSD is the relative standard deviation in percent.

Contact duration (mn)	Blank (step 1)	RSD (%)	Ferrofluid (step 2)	RSD (%)	Concentrated HCl rinsing (step3)	RSD (%)
3	2.31	0.42	41	0.80	5.5	1.42
10	0.966	1.42	20	1.12	4.13	1.42
30	1.79	1.41	19.8	0.46	4.76	0.97

simplify error propagation. The error varies between 0.3% and 2.5% depending on the samples.

Less than 20 ppt of iron is detected in the ultrapure water used. Suprapur 30% HCl is used, new plastic tubes for samples and plastic cones with pipettes, all tested to bring a negligible contribution to the iron content detected. Dilutions are done directly in the final tube, by weighting to avoid flasks and other intermediates.

The raw results obtained at the three steps described in the main text are given in Table S1. These values are then converted into a total mass m_{ox} of iron oxide in the sample using the total mass of the given sample analyzed, and a density of 5 g/cm^3 for the iron oxide Fe_2O_3. Considering the average NPs diameter to be 8 nm, the mass of one NP is $M_{NP} = 1.34\ 10^{-18}$ g and the corresponding surface occupied by one NP on a disk is $S_{NP} = 5.0310^{-13}$ cm^2. Therefore the coverage θ is estimated as $\theta = m_{ox}/M_{NP} * S_{NP}/S_{Pt}$ where $S_{Pt} = 0.3$ cm^2 is the surface of platinum electrode exposed to the colloidal dispersion in the cell. The converted results are given in Table 2 of main text.

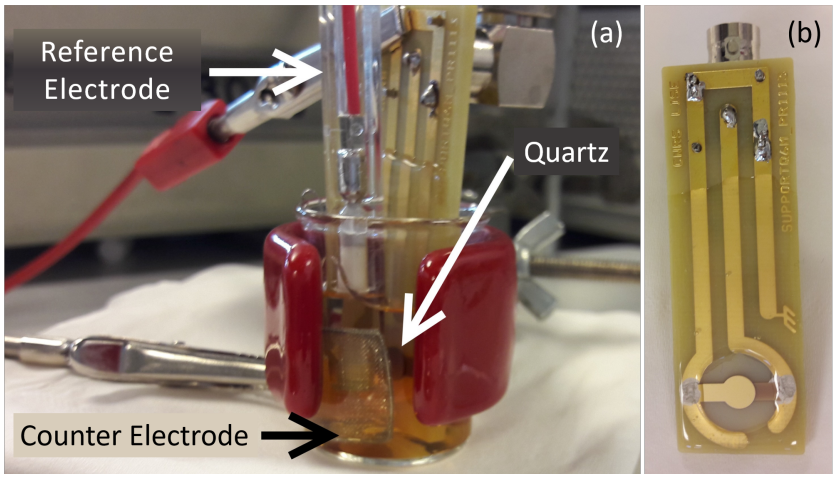


Figure S1. (a) EQCM device with a diluted ferrofluid solution. The reference electrode is a saturated calomel electrode and the counter electrode is a platinum grid. (b): gold coated quartz used for microbalance measurements. The connections for the application of potential are also visible.

S3. QCM measurements

S3.1. Sauerbrey model

A Quartz Crystal Microbalance measurement can allow determination of the quantity of adsorbed particles on the quartz, provided that the NPs are firmly and uniformly adsorbed on the quartz and that the induced variation Δf of the fundamental frequency f of the quartz is less than 10%. The variation of mass Δm of the vibrating crystal is then related to the variation of the fundamental frequency of the quartz Δf by the Sauerbrey equation [6]:

$$\Delta f = \frac{-2f^2}{\rho c}\frac{\Delta m}{A} \tag{S1}$$

with ρ = 2648 kg/m^3 the density of quartz, c is the speed of sound in the quartz and A the quartz area covered by each of the electrodes. For a resonant frequency of about 9 MHz, the mass variation associated with a frequency decrease of 1 Hz is therefore

$$\frac{\rho c}{2f^2} = 5.5\ \mathrm{ng/cm^2} \tag{S2}$$

S3.2. Principle of EQCM measurements

The principle of the measurements carried out therefore consists of studying the mass per unit area adsorbed on the quartz according to the type of aqueous ferrofluid (changing the nature of interfacial species), the electrode metal (quartz covered by gold or platinum) and the potential applied to the electrode. The potential is applied by means of a three-electrode arrangement (see S1-a : the metal covering the quartz constitutes the working electrode, the counter electrode is a platinum grid and the reference electrode is a saturated calomel electrode (ECSaq). The potential is applied between the working electrode and the reference electrode using a potentiostat (SotelemPGSTAT).

S3.3. Validation of gold microbalance measurements/ Experimental device

In order to verify the validity of the device used, the results of Lucas and co-authors[7] are reproduced here studying by EQCM the adsorption of maghemite nanoparticles in an acid medium on a gold surface (see also [9]). To do this, the quartz used is covered with a thin layer of gold (see S1-b). The chosen ferrofluid is a dispersion in nitric acid medium, with sample characteristics close to the FF in perchloric acid medium used by Lucas and co-authors.

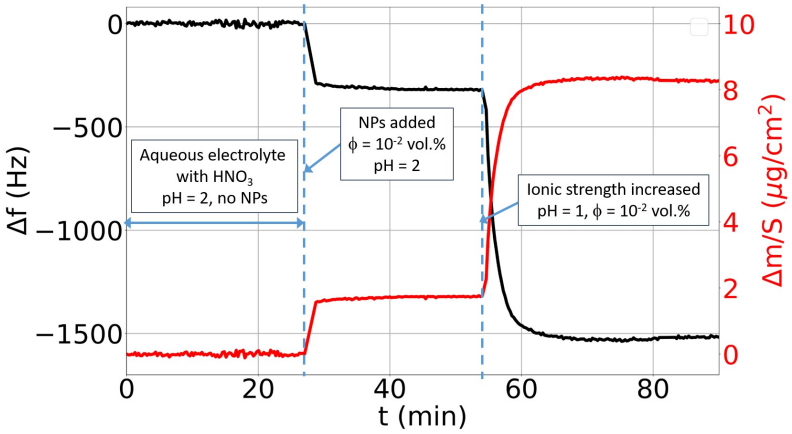


Figure S2. Open circuit QCM measurements on gold electrode as a function of ionic strength for acidic FF. The frequency variation is shown on the left-hand y-axis in black and the corresponding ground variation is shown on the right-hand y-axis in red. Initially the solution contains no nanoparticles and has a pH of 2 (ionic strength $I = 10^{-2}$M). The nanoparticles are added at 27 minutes to the volume fraction $\phi = 10^{-2}$% at constant pH. Around 55 minutes, the pH is changed to 1 (ionic strength $I = 10^{-1}$M).

S3.4. Effect of ionic strength

The QCM measurements show the adsorption of acidic nanoparticles on the gold surface at $pH = 2$ (see S2). This adsorption is rather fast, of the order of a few minutes, and saturated at a value, in accordance with Lucas' results presented earlier [8]. The influence of the ionic strength is also highlighted. Once the plateau at $pH = 2$ is reached, the solution is acidified while keeping the concentration of nanoparticles constant, the adsorbed mass increases considerably, by a factor of approximately 5, reaching $8.3\mu g/cm^2$. The shielding

effect linked to the ionic strength of the electrostatic repulsion between the free (non-adsorbed) particles in solution and those already adsorbed, which was highlighted by [8], is thus regained.

S3.5. Effect of potential

The effect of the potential of the gold electrode on the adsorption of nanoparticles is also measured. The application of a positive potential, up to + 0.8 V relative to ECSaq, to positively charge the surface, which has the same sign as the nanoparticles, has no measurable effect. If this potential is applied before and during the addition of the particles, adsorption is still observed. If it is applied after particles are already adsorbed, no further desorption or adsorption is measured. This result confirms that the electrostatic interactions between the electrode and the nanoparticles are not preponderant here.

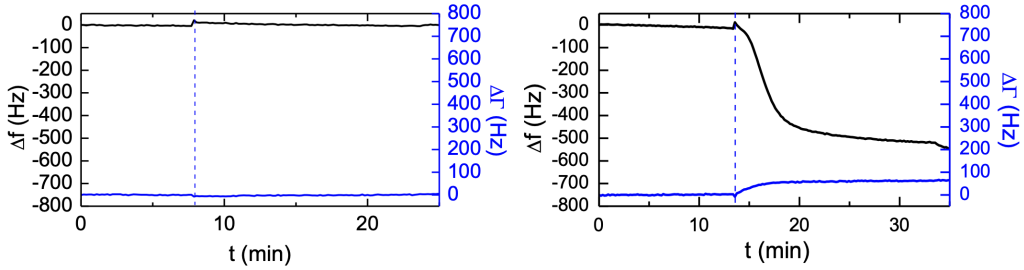


Figure S3. QCM measurements of on platinum electrode as a function of ionic strength for dispersions of citrate-coated NPs (ferrofluids) - associated to Fig. 13 of main paper - Comparison between the resonant frequency variations, Δf, and the dissipation variations, $\Delta\Gamma$, over time. The nanoparticles are added after about ten minutes. (left): $\phi = 2.8\ 10^{-3}\%$ and tetrabutylammonium citrate concentration of 5 mM; (right): $\phi = 10^{-2}\%$ and concentration of tetrabutylammonium citrate of 30 mM.

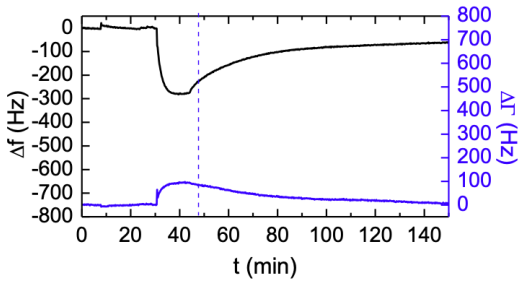


Figure S4. QCM measurements of on platinum electrode for dispersions of citrate-coated NPs (ferrofluids) - associated to Fig. 14 of main paper - Comparison between the resonant frequency variations, Δf, and the dissipation variations, $\Delta\Gamma$, over time. $\phi = 2.8\ 10^{-3}\%$ and tetrabutylammonium citrate concentration of 5 mM; (right):

S3.6. QCM measurements with colloidal dispersions of maghemite nanoparticles

A network analyzer (Agilent 4194A) was used to conduct the electroacoustic measurements. An equivalent BVD (Butterworth-Van Dyke) circuit was automatically obtained around the resonant frequency of the device. The values of R, L, C obtained from this equivalent circuit were used to calculate the resonant frequency of the microbalance, f, and the half width at half-height of the conductance peak, Γ, using the following equations:

$$f = \frac{1}{2\pi\sqrt{LC}} \tag{S3}$$

$$\Gamma = \pi f^2 RC \tag{S4}$$

Therefore both Δf and $\Delta\Gamma$ can be obtained as a function of time. They are plotted in S3 and S4. They are associated to the measurements of Fig. 13 and 14 of main text. $\Delta\Gamma$ variations are small or negligible with respect to that of the resonant frequency Δf. It confirms the hypothesis that the maghemite nanoparticles are firmly attached to the quartz crystal during QCM measurements.

S3.7. Validation of the measuring device

All the effects observed by Lucas and co-authors for maghemite nanoparticles in an acid environment on gold surface are verified with the device used here; Namely – the adsorption of the particles on the metal surface increase with the ionic strength, – the number of nanoparticles adsorbed at saturation and – an absence of influence of the electrode potential on the adsorption phenomena.

The homogeneity of the particle adsorption across the electrode surface is 'assumed' based on the observation by Lucas et al., (ref. 48, see Figure 1 within) where a uniform distribution of iron oxide nanoparticles was revealed by the Atomic Force Microscopy measurements on a gold surface. These results validate the quartz microbalance system for demonstrating the adsorption of nanoparticles on a platinum electrode by a ferrofluid at $pH = 7$ as shown in the main text.

1. Bacri, J.C.; Perzynski, R.; Salin, D.; Cabuil, V.; Massart, R., Ionic ferrofluids: A crossing of chemistry and physics. *J. Magnetism and Magnetic Materials* **1990** 85, 27-32; DOI 10.1016/0304-8853(90)90010-N.
2. Filomeno, C.L.; Kouyaté, M.; Peyre, V. ; Demouchy, G. ; Campos, A.F.C.; Perzynski, R.; Tourinho, F.A.; Dubois, E., Tuning the solid/liquid interface in ionic colloidal dispersions: Influence on their structure and thermodiffusive properties. *J.Phys.Chem. C* **2017** 121, 5539-5550; DOI: 10.1021/acs.jpcc.6b10280
3. Kouyaté, M. ; Filomeno, C.L.; Demouchy, G.; Mériguet, G.; Nakamae, S.; Peyre, V.; Roger, M.; Cebers, A.; Depeyrot, J.; Dubois, E.; Perzynski, R., Thermodiffusion of citrate-coated γ-Fe_2O_3 nanoparticles in aqueous dispersions with tuned counter-ions – anisotropy of the Soret coefficient under a magnetic field *Phys. Chem. Chem. Phys.* **2019** 21, 1895-1903; DOI: 10.1039/c8cp06858e
4. Salez Thomas J., Huang B.T., Rietjens M., Bonetti M., Wiertel- Gasquet C., Roger M., Filomeno C.L., Dubois E., Perzynski R., Nakamae S., Can charged colloidal particles increase the thermoelectric energy conversion efficiency? *Phys. Chem. Chem. Phys.* **2017** 19, 9409–9416; DOI: 10.1039/C7CP01023K.
5. Filomeno, C; Fiuza, T.; Kouyaté, M.; Riedl, J.C.; Sarkar, M.; Demouchy, G.; Depeyrot, J.; Dubois, E.; Mériguet, G.; Perzynski, R.; Peyre, V.; Chapter 5 in *Material Aspects of Ferrofluids*, CRC Press, Taylor & Francis Group, R.P. Pant, Vidya Nand Singh, Komal Jain, Arvind Gautam edn, **2023**, pp. 94–115; DOI: 10.1201/9781003274247-5.
6. Sauerbrey G., Verwendung von schwingquarzen zur wägung dünner schichtenund zur mikrowägung. *Zeitschrift für Physik* **1959** 155, 2, pp 206–222. DOI: 10.1007/BF01337937
7. Lucas I.T., Dubois E., Chevalet J., Durand-Vidal S., Reactivity of nanocolloidal particles γ-Fe_2O_3 at the charged interfaces Part 1. The approach of particles to an electrode. *Physical Chemistry Chemical Physics* **2008** 10, 22, pp 3263–3273. DOI:10.1039/b718593f
8. Lucas I.T., Reactivity of nanoparticles at charged interfaces : Electronic transfer in colloidal suspension and electrokinetic phenomena at the nanometric scale. *PhD Thesis Université Pierre et Marie Curie - Paris VI*, Sept. 2007.
9. Salez, T. J. *Effets thermoélectriques dans des liquides complexes : liquides ioniques et ferrofluides*. PhD thesis, Université Paris sciences et lettres, Paris, France, 2017. Available at: https://theses.hal.science/tel-01968050.